Attention rhythmically shapes sensory tuning

Laurie Galas[1,*], Ian Donovan[2,*], Laura Dugué[1,3]

Affiliations

[1]Université Paris Cité, CNRS, Integrative Neuroscience and Cognition Center, F-75006 Paris, France

[2]Department of Psychology and Center for Neural Science, New York University, NY 10003 New York, USA

[3]Institut Universitaire de France (IUF), Paris, France

*L.G. and I.D. contributed equally to this work.

Corresponding Author

Laurie Galas

laurie.galas@etu.u-paris.fr

Conflict of interest

The authors declare no competing financial interests.

Acknowledgements

This project has received funding from the European Research Council (ERC) under the European Union's Horizon 2020 research and innovation programme (grant agreement No 852139 - Laura Dugué). We also thank Laetitia Grabot and Kirsten Petras for their useful comments on the manuscript and advice on analyses.

Summary

The rhythmic sampling theory of attention, stating that attention periodically samples information at low frequencies (<20Hz), has become an important topic of research[1–4], with a surge of studies finding rhythmic fluctuations of behavioral performance (reaction time, d-prime, accuracy) in various sensory modalities (vision[5–9], audition[10,11], somatosensation[12]) and types of behavioral response (finger, hand, arm, eye movements[13–15]). Yet, the existence, and thus, functional significance of such rhythmic behavior remains largely debated, due to a combination of complex and controversial methodological procedures, as well as the lack of understanding of the functional (sensory) mechanism underlying such rhythms. Here, we specifically assess the link between behavioral rhythms and sensory representations. In a ~22-hour behavioral experiment, participants (n=15) performed a dual task in which covert, spatial (sustained and exploratory) attention was manipulated, and then probed at various delays during the task. Our results show that sustained attention samples information periodically at ~12Hz (alpha), while exploratory attention reorients from one stimulus to another at ~6Hz (theta). Critically, reverse correlation analyses[16–20] show that the alpha sustained-attention rhythm reflects both increased suppression of distracting features and increased gain to task-relevant stimulus feature (orientation). Together these two processes keep the influence of relevant stimulus information constant over time while improving performance (periodically) via noise reduction. The theta exploratory-attention rhythm, however, is only associated with changes in the gain around the task-relevant stimulus feature. Our study goes beyond rhythms quantification and demonstrates how attention rhythmically shapes sensory representations.

Keywords

Alpha, Attention, Behavioral rhythms, Gain, Noise suppression, Sensory representations, Theta

Results

Attention allows selective facilitation of sensory information processing, efficiently allocating resources based on task demands[21–23]. When voluntarily deployed, (endogenous) attention's influence on perception and behavior can be sustained at will, benefiting performance for long periods of time. Although this classic understanding of sustained attention is well established, a growing body of evidence converges toward a more complex dynamic: attention periodically samples information, across both time and spatial locations[1–4]. Specifically, rhythmic fluctuations in performance due to attention suggest that sensory information processing alternates between periods of greater (when in the attention spotlight) and lesser (when outside) facilitation. This view has been recently challenged[3,4,24–27] notably based on considerations regarding protocols (e.g., low number of trials[27], low sampling frequency resolution[3] and analysis procedures[26]; but see[25,28,29]). Additionally, there remains a lack of evidence for the specific sensory mechanism underlying variations in behavioral performance. Here we address these issues by designing a protocol for measuring periodic fluctuations of attentional performance in individual participants (with a large number of trials), and using an analysis procedure well-suited to assess potential fluctuations in sensory representations.

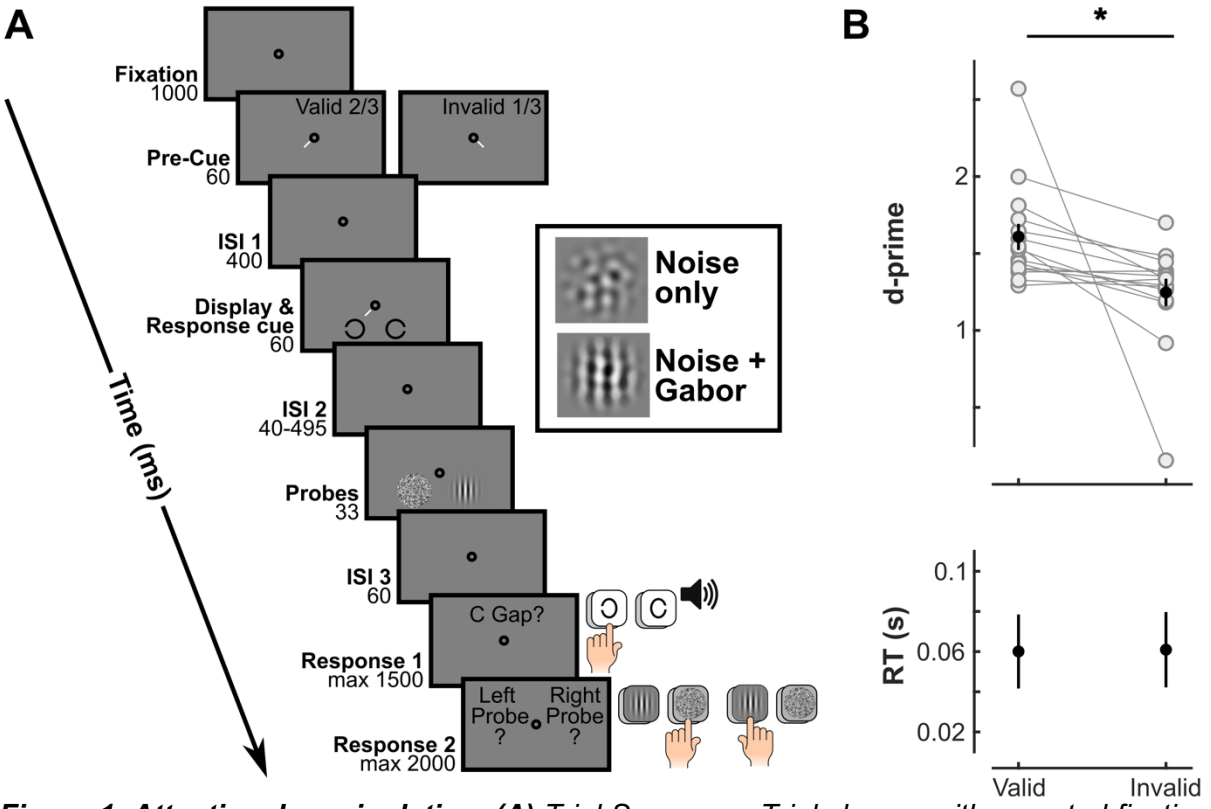

Figure 1. Attentional manipulation. (A) *Trial Sequence. Trials began with a central fixation period of 1000ms. An endogenous pre-cue appeared for 60ms. After 400ms, Landolt-Cs were displayed for 60ms together with a response cue indicating which Landolt-C was the target (2/3 of Valid trials, i.e., target at pre-cued location). Each Landolt-C could be oriented to the right or to the left randomly. After a variable delay from 40ms to 495ms (35ms step; only the fixation circle remained on the screen), two patches were presented for 33ms at the same location as the Landolt-C. Each patch could either show noise only (1/2 of trials) or noise + Gabor (1/2). After a third ISI of 60ms, participants were instructed to report: (1) the orientation of the target Landolt-C (right/left; discrimination task), and (2) the presence or absence of a Gabor in each of the two patches.* ***(B)*** *Behavioral results of the discrimination task. Individual (gray) and averaged (black) d-primes and median reaction times (RT) in the valid and invalid conditions. Error bars: standard error of the mean. *: significant difference between valid and invalid trials (p=0.034).*

We used a well-established psychophysics protocol (**Figure 1A**) tailored to identifying rhythms in attentional tasks[8,30,31] (for review[3]). Covert, voluntary attention was manipulated using a pre-cue (2/3 validity). Participants (n=15) were instructed to first perform a discrimination task (by indicating the side of the gap, left or right, of a target Landolt-C) allowing us to confirm that attention was successfully manipulated and deployed to the cued location (**Figure 1B**). D-prime was significantly higher for valid (target at the cued location) than invalid (target at the uncued location) trials (paired-sample two-tailed t-test: $t(14) = 2.34$, p-value = 0.034, Cohen's $d = -1.07$). Reaction times were similar for valid and invalid trials ($t(14) = -0.83$, p-value = 0.418, Cohen's $d = 0.02$), indicating no speed-accuracy trade-off.

In the same trial, after a variable delay, participants were presented with a second target, on which they were asked to perform a detection task reporting the presence or absence of a vertical Gabor embedded in band-passed noise. The noise had random orientation content, drawn from a uniform distribution across all orientations -90 to +90 degrees (polar angle) and a spatial frequency of 3 cycles per degree (cpd). On half of the trials, a Gabor (3 cpd sinusoidal grating in an envelope subtending 2º; oriented vertically) was embedded in the noise patch. This second task was used to probe attention at each of the two stimulus locations and at various times during attentional orienting (valid trials; sustained attention) and reorienting (invalid; exploratory attention), assessing potential rhythms in attentional sampling.

We computed d-primes for this detection task independently for the valid and invalid conditions and for each ISI between the discrimination and probes onset. Across ISIs, d-prime exhibited multiple peaks and troughs, and individual data makes clear this was highly consistent across participants (**Figure 2A**). We then performed fast-fourier transforms (FFT) of the averaged d-primes for the valid and invalid conditions separately. Peak frequencies were identified: 12.3Hz in valid and 6.1Hz in invalid (permutations tests: 100,000 surrogates, $p = 0.05$; **Figure 2B**). Note that in the invalid condition, an additional significant peak frequency was observed at 2.04Hz reflecting the inverted U-shape trend (no detrending was performed here, see[7,31]; we did not analyze it further). We also showed that the 12.3Hz (for the valid condition) and 6.1Hz (for the invalid) individual periodic modulations were in phase across participants (Rayleigh tests for circular data showed significant non-uniform distributions for both valid: $Z = 9.75$, $p = 9.04 \times 10^{-6}$; and invalid: $Z = 4.22$, $p = 0.012$).

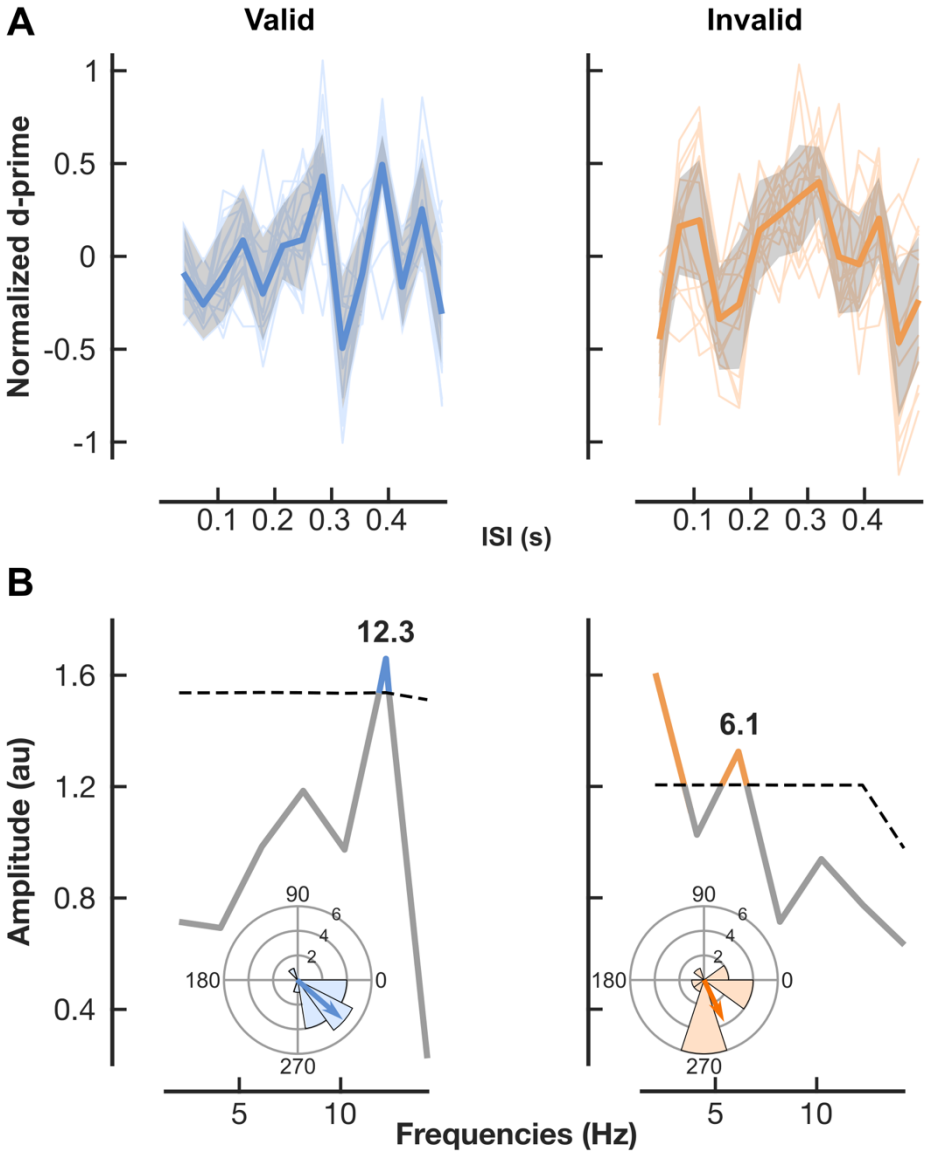

Figure 2. Behavioral rhythms. (A) *Individual (light traces) and averaged (dark traces) d-prime time-courses (n=15) for valid (blue) and invalid (orange) conditions separately. Shaded area: 95% confidence interval.* ***(B)*** *Amplitude spectra obtained from FFT of d-primes time course averaged across participants. Dotted line: p=0.05 (permutation test). Polar histogram of individual phases (light bins) and weighted phase averages (arrows) at 12.3Hz in the valid condition and 6.1Hz in the invalid condition.*

For valid and invalid conditions separately, we split the ISI into low- and high-performance ISIs. ISIs corresponding to d-prime local maxima (and which were above the averaged d-prime time-courses) were categorized as *high-performance* and ISIs corresponding to d-prime local minima (and which were below the average) were categorized as *low-performance*. We then combined all high-performance trials (coming from 4 different ISIs in valid: 145, 285, 390 and 460ms; 3 ISIs in invalid: 110, 320 and 425ms) and low-performance trials (5 ISIs in valid: 75, 180, 320, 425 and 495ms; 4 ISIs in invalid: 40, 145, 390 and 460ms) for the next analysis.

Subsampling (100 repetitions) was performed to equalize the number of trials between valid and invalid, and high- and low-performance conditions. This trial separation was then used to assess modulations in sensory representations using reverse correlation analysis.

Fluctuations in sensitivity (d-prime) suggest a modification of sensory representations over time, such that high performance should be associated with more optimal sensory tuning compared to low performance. Here we assess which characteristics of sensory representations varied. If sensory tuning is modeled as a Gaussian distribution across orientations (**Figure 3**), tuning can vary via differences in: **(A)** tuning sharpness or variance: for high-performance trials, the perception would present a sharper tuning to the relevant elements for the task; **(B)** gain or amplitude: for high-performance trials, there would be a higher gain for the relevant information for the task; and **(C)** suppression or baseline shift: for high-performance trials, there would be a decrease in the baseline, i.e., suppression of irrelevant information for the task.

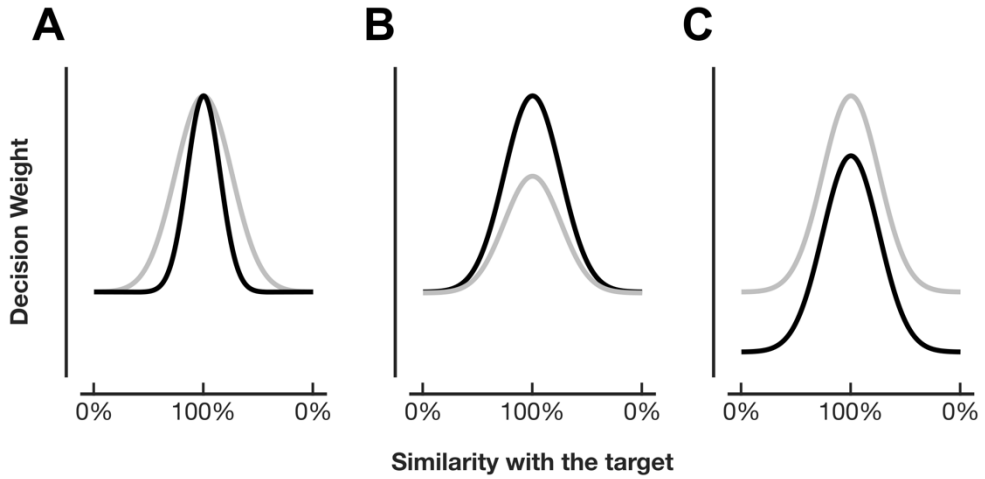

Figure 3. Sensory tuning hypotheses. *Gaussian model of participant's sensory tuning. Sensory representations are different during phases of high (black traces) versus phases of low (gray traces) performance. Modifications in the* ***(A)*** *tuning sharpness,* ***(B)*** *tuning amplitude (gain),* ***(C)*** *tuning baseline.*

Reverse correlation of behavioral performance (see **STAR Methods**) allowed testing of these three hypotheses, separately for each attention condition – sustained (valid) and exploratory (invalid). To infer the underlying sensory representation from the behavioral responses, we regressed the stimulus energy (i.e., visual resemblance of the noise to a range of orientation values) across trials –separately for high- and low-performance trials– with each participant's

responses using a binomial regression. This provided a sensitivity kernel for each orientation, i.e., β (or decision) weight, representing the level of correlation between the proportion of trials reporting "Target Present" and the energy of that particular orientation in the noise of the stimulus (**Figure 4**; Note that decision weights were averaged for positive and negative orientations). A high decision weight indicates a high correlation, suggesting that more energy for the orientation value in question within the noise positively influenced the likelihood of "Target Present" responses. The results first show that the highest decision weights were observed for orientation corresponding to the target grating orientation (0°; peak of the Gaussian). For each orientation, a paired t-test on the difference between high- and low-performance trials' decision weights was then computed and Bonferroni corrected for 13 comparisons (p-threshold Bonferroni corrected = 0.0038; positive and negative orientation results were averaged). We observed significant differences for the values far from the target orientation mainly in the valid condition, and for near-target values in the invalid condition.

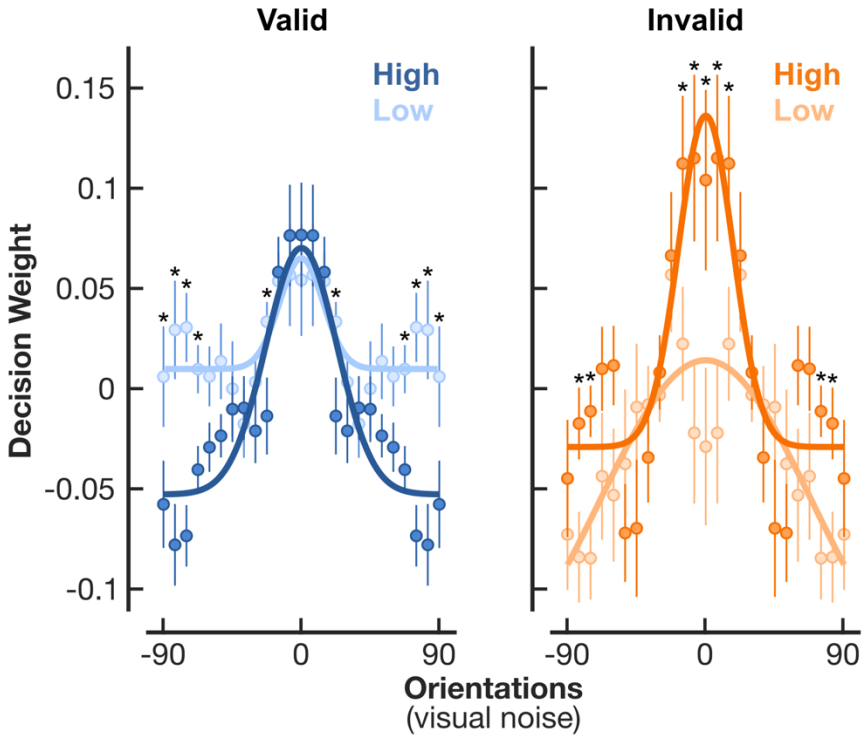

Figure 4: Decision weight from reverse correlation for valid and invalid trials. *Dark traces: high-performance trials. Light traces: low-performance trials. Circles: average weight across participants of the correlation between energy at each orientation (averaged across positive and negative orientations) and participant's response using a GLM. Error bars: 95% confidence interval. Solid lines: Gaussian fit. *: significant difference between high- and low-performance (p-threshold Bonferroni corrected = 0.0038).*

We then fitted a single gaussian curve –the tuning curve– to the 25 decisions weights (1 per orientation; see **STAR methods**). To identify the changes in tuning that accompany periodicity in d-prime, we compared, across participants, the three following free parameters in the tuning fits: standard deviation (SD), amplitude and baseline, between high-performance and low-performance trials, separately for the valid and invalid conditions. There was no significant difference between high- and low-performance trials in both valid and invalid conditions for the SD (valid: $t(14) = 1.14$, $p = 0.274$ estimate = 9.27 ± 8.14, standard error; invalid: $t(14) = -0.12$, $p = 0.903$, estimate = -1.07 ± 8.71). Amplitude was significantly higher in high- compared to low-performance trials in both valid and invalid conditions (valid: $t(14) = -3.76$, $p = 0.002$, estimate = -0.08 ± 0.02; invalid: $t(14) = -4{,}23$, $p = 0.001$, estimate = -0.11 ± 0.03). Baseline was significantly lower in high- compared to low-performance trials for the valid condition only (valid: $t(14) = 6.96$, $p = 0$, estimate = 0.07 ± 0.01; invalid: $t(14) = -1.51$, $p = 0.153$, estimate = -0.03 ± 0.02). These results suggest that, in the valid condition, when the attention was sustained at one location, the performance fluctuation at alpha frequency is mediated by rhythmic enhancement (gain) of relevant features and suppression of distracting features (baseline) (**Figure 3**, hypotheses B and C); whereas, in the invalid condition, when attention had to explore the space, we observed fluctuation at theta frequency mediated exclusively by a rhythmic change in enhancement (gain) of relevant features (**Figure 3**, hypothesis B).

Discussion

The rhythmic sampling theory of attention has become an important topic of research, yet remains largely debated due to methodological considerations, as well as a lack of clear understanding regarding the sensory mechanism underlying performance fluctuations. Here we addressed this critical gap using a psychophysics paradigm with a large amount of data collected for each participant, and applying reverse correlation analysis correlating stimulus energy of irrelevant noise with behavioral detection performance. We assessed the fluctuations in sensory representations for two voluntary attention modes, i.e., sustained and exploratory.

First, we showed that performance fluctuated periodically at the alpha frequency (12.3Hz) for sustained attention and theta frequency (6.1Hz) for exploratory attention, replicating previous reports[8,9,32,33]. Such effects were further observed for each individual participant. Second, reverse correlation analysis revealed differences in feature tuning across time between the two attention modes. Sustained attention displayed rhythmic suppression of distracting features (while keeping the gain constant). Exploratory attention exclusively showed enhancement (gain) of relevant features. Together, these results confirm attention-specific rhythms of behavioral performance, and go beyond by demonstrating specific underlying sensory mechanisms.

Previous decades of attention research have concentrated on the general effects of attention on perceptual performance and showed a wealth of evidence for both signal enhancement of task-relevant stimulus features and external noise reduction. Authors have notably demonstrated that attention can enhance signals through contrast gain (e.g., [34–37]), response gain (e.g., [36,37]), orientation sensitivity gain (e.g., [35,38]), spatial resolution gain (e.g., [39–42]) or information processing speed gain (e.g., [43]). Such enhancement could occur for targets presented below, above or at threshold. Similarly, active suppression of irrelevant information, also called external noise reduction, would occur both for targets presented suprathreshold and near-threshold[44–51]. Given the accumulated evidence for both attentional mechanisms (enhancement and suppression), they are almost certainly not mutually exclusive. Dosher and Lu[52] indeed showed that either mechanism can arise in the same task under different levels of task difficulty: with fewer distractor locations or low external noise, there is a stronger signal enhancement effect; and with more distractor locations or higher external noise, there is a stronger external noise reduction effect. Others have also argued that which of the two mechanisms is engaged depends on the type of attention deployed. For instance, while endogenous (voluntary) attention is more often linked to external noise reduction, exogenous (involuntary) attention is linked to both external noise reduction and signal enhancement[53].

Here we used reverse correlation of behavioral performance to assess feature tuning across time and attention modes, which d-prime measures alone are not directly capable of. While

signal enhancement was observed for both sustained and exploratory attention modes, the suppression of irrelevant features, analogous to external noise reduction, was only observed for sustained attention. Specifically, when attention was directed to the target location –valid condition– attention suppressed irrelevant features far from the target orientation (baseline shift), and then compensated with an increase in gain (amplitude). This resulted in equal decision weights at and near the target feature for both high- and low-performance phases of d-prime sensitivity, but lower decision weights far from the target orientation. In other words, when attention is oriented and sustained at a target location, alpha rhythms in performance are primarily due to fluctuations in the suppression of irrelevant stimulus features – advantageous suppression at peaks and poorer suppression at troughs– while a gain mechanism keeps the influence of relevant stimulus information constant over time. When attention is instead reoriented from an irrelevant location to a relevant one –invalid condition– theta rhythms in behavioral sensitivity are associated only with changes in the amplitude of the tuning function, most strongly influencing sensitivity around the target feature, such that high-performance phases have higher decision weights at orientations close to target feature compared to low-performance phases.

Notably, we found external noise reduction and signal enhancement in separate modes of voluntary spatial attention –sustained and exploratory, respectively–, while difficulty remained constant, as both attention conditions shared the same number of targets, locations, and distractors, as well as the same level of stimulus noise. We speculate that the pattern of our findings is related to the distinct functional roles of the sustained and exploratory modes of attention. In other words, because attention efficiently allocates resources based on task demands[21–23], finding distinct behavioral tradeoffs during different modes of attention suggests the two modes have distinct roles in aiding perception and performance. On the one hand, when attention shifts from one location to another, i.e., attention is exploring space, signal enhancement of the most relevant features may aid in locating the target, which is necessary before it can be examined and discriminated. On the other hand, when attention is sustained on a single location, i.e., the target location has already been identified, perception is enhanced

249 via external noise reduction, as it is no longer necessary to find the target via signal
250 enhancement.
251 Further, the particular frequency of either sensory tuning modulation may be related to their
252 corresponding attention modes' respective functional roles (see reviews[3,33]). Alternatively,
253 sensory mechanism may operate necessarily at a particular frequency due to metabolic or
254 neural processing constraints. The link between attention mode, the respective frequencies of
255 performance modulation, and the underlying sensory tuning mechanisms is a topic in need of
256 further investigation.

References

1. VanRullen, R. (2016). Perceptual Cycles. Trends Cogn. Sci., *20*, 723–735. 10.1016/j.tics.2016.07.006.
2. Fiebelkorn, I.C., and Kastner, S. (2019). A Rhythmic Theory of Attention. Trends Cogn. Sci., *23*, 87–101. 10.1016/j.tics.2018.11.009.
3. Kienitz, R., Schmid, M.C., and Dugué, L. (2022). Rhythmic sampling revisited: Experimental paradigms and neural mechanisms. Eur. J. Neurosci., *55*, 3010–3024. ejn.15489. 10.1111/ejn.15489.
4. Keitel, C., Ruzzoli, M., Dugué, L., Busch, N.A., and Benwell, C.S.Y. (2022). Rhythms in cognition: The evidence revisited. Eur. J. Neurosci., *55*, 2991–3009. 10.1111/ejn.15740.
5. Dugué, L., Marque, P., and VanRullen, R. (2015). Theta Oscillations Modulate Attentional Search Performance Periodically. J. Cogn. Neurosci., *27*, 945–958. 10.1162/jocn_a_00755.
6. Landau, A.N., and Fries, P. (2012). Attention Samples Stimuli Rhythmically. Curr. Biol., *22*, 1000–1004. 10.1016/j.cub.2012.03.054.
7. Fiebelkorn, I.C., Saalmann, Y.B., and Kastner, S. (2013). Rhythmic Sampling within and between Objects despite Sustained Attention at a Cued Location. Curr. Biol., *23*, 2553–2558. 10.1016/j.cub.2013.10.063.
8. Senoussi, M., Moreland, J.C., Busch, N.A., and Dugué, L. (2019). Attention explores space periodically at the theta frequency. J. Vis., *19*, 1–17. 10.1167/19.5.2.
9. Dugué, L., Xue, A.M., and Carrasco, M. (2017). Distinct perceptual rhythms for feature and conjunction searches. J. Vis., *17*, 1–15. 10.1167/17.3.22.
10. VanRullen, R., Zoefel, B., and Ilhan, B. (2014). On the cyclic nature of perception in vision versus audition. Philos. Trans. R. Soc. Lond., B, Biol. Sci., *369*, 20130214. 10.1098/rstb.2013.0214.
11. Ho, H.T., Burr, D.C., Alais, D., and Morrone, M.C. (2019). Auditory Perceptual History Is Propagated through Alpha Oscillations. Curr. Biol., *29*, 4208–4217. 10.1016/j.cub.2019.10.041.
12. Baumgarten, T.J., Schnitzler, A., and Lange, J. (2015). Beta oscillations define discrete perceptual cycles in the somatosensory domain. Proc. Natl. Acad. Sci. USA, *112*, 12187–12192. 10.1073/pnas.1501438112.
13. Benedetto, A., and Morrone, M.C. (2019). Visual sensitivity and bias oscillate phase-locked to saccadic eye movements. J. Vis., *19*, 1–16. 10.1167/19.14.15.
14. Kienitz, R., Schmiedt, J.T., Shapcott, K.A., Kouroupaki, K., Saunders, R.C., and Schmid, M.C. (2018). Theta Rhythmic Neuronal Activity and Reaction Times Arising from Cortical Receptive Field Interactions during Distributed Attention. Curr. Biol., *28*, 2377–2387. 10.1016/j.cub.2018.05.086.
15. Chota, S., Luo, C., Crouzet, S.M., Boyer, L., Kienitz, R., Schmid, M.C., and VanRullen, R. (2018). Rhythmic fluctuations of saccadic reaction time arising from visual competition. Sci. Rep., *8*, 15889. 10.1038/s41598-018-34252-7.
16. Ahumada, A.J., Jr. (2002). Classification image weights and internal noise level estimation. J. Vis., *2*, 121–131 10.1167/2.1.8.
17. Eckstein, M.P., Shimozaki, S.S., and Abbey, C.K. (2002). The footprints of visual attention in the Posner cueing paradigm revealed by classification images. J. Vis. *2*, 3. 10.1167/2.1.3.
18. Paltoglou, A.E., and Neri, P. (2012). Attentional control of sensory tuning in human visual perception. J. Neurophysiol., *107*, 1260–1274. 10.1152/jn.00776.2011.
19. Wyart, V., Nobre, A.C., and Summerfield, C. (2012). Dissociable prior influences of signal probability and relevance on visual contrast sensitivity. Proc. Natl. Acad. Sci. USA, *109*, 3593–3598. 10.1073/pnas.1120118109.
20. Li, H.-H., Barbot, A., and Carrasco, M. (2016). Saccade Preparation Reshapes Sensory Tuning. Curr. Biol., *26*, 1564–1570. 10.1016/j.cub.2016.04.028.
21. Lennie, P. (2003). The cost of cortical computation. Curr. Biol., *13*, 493–497. 10.1016/s0960-9822(03)00135-0.
22. Carrasco, M. (2011). Visual attention: The past 25 years. Vision Res., *51*, 1484–1525.

10.1016/j.visres.2011.04.012.
23. Merholz, G., Grabot, L., VanRullen, R., and Dugué, L. (2022). Periodic attention operates faster during more complex visual search. Sci. Rep., *12*, 6688. 10.1038/s41598-022-10647-5.
24. Ruzzoli, M., Torralba, M., Morís Fernández, L., and Soto-Faraco, S. (2019). The relevance of alpha phase in human perception. Cortex, *120*, 249–268. 10.1016/j.cortex.2019.05.012.
25. Fiebelkorn, I.C. (2022). Detecting attention-related rhythms: When is behavior not enough? (Commentary on van der Werf et al. 2021). Eur. J. Neurosci., *55*, 3117–3120. 10.1111/ejn.15322.
26. Brookshire, G. (2022). Putative rhythms in attentional switching can be explained by aperiodic temporal structure. Nat. Hum. Behav., *6*, 1280–1291. 10.1038/s41562-022-01364-0.
27. van der Werf, O.J., Ten Oever, S., Schuhmann, T., and Sack, A.T. (2022). No evidence of rhythmic visuospatial attention at cued locations in a spatial cuing paradigm, regardless of their behavioural relevance. Eur. J. Neurosci., *55*, 3100–3116. 10.1111/ejn.15353.
28. Fiebelkorn, I.C. (2022). There Is More Evidence of Rhythmic Attention than Can Be Found in Behavioral Studies: Perspective on Brookshire, 2022. J. Cogn. Neurosci., *35*, 128–134. 10.1162/jocn_a_01936.
29. Re, D., Tosato, T., Fries, P., and Landau, A.N. (2022). Perplexity about periodicity repeats perpetually: A response to Brookshire. Preprint at bioRxiv, 10.1101/2022.09.26.509017.
30. Dugué, L., McLelland, D., Lajous, M., and VanRullen, R. (2015). Attention searches nonuniformly in space and in time. Proc. Natl. Acad. Sci. USA, *112*, 15214–15219. 10.1073/pnas.1511331112.
31. Michel, R., Dugué, L., and Busch, N.A. (2022). Distinct contributions of alpha and theta rhythms to perceptual and attentional sampling. Eur. J. Neurosci., *55*, 3025–3039. 10.1111/ejn.15154.
32. Dugué, L., Beck, A.-A., Marque, P., and VanRullen, R. (2019). Contribution of FEF to Attentional Periodicity during Visual Search: A TMS Study. eNeuro *6*, ENEURO.0357-18.2019. 10.1523/ENEURO.0357-18.2019.
33. Dugué, L., and VanRullen, R. (2017). Transcranial Magnetic Stimulation Reveals Intrinsic Perceptual and Attentional Rhythms. Front. Neurosci., *11*, 154. 10.3389/fnins.2017.00154.
34. Cameron, E.L., Tai, J.C., and Carrasco, M. (2002). Covert attention affects the psychometric function of contrast sensitivity. Vision Res., *42*, 949–967. 10.1016/S0042-6989(02)00039-1.
35. Lee, D.K., Itti, L., Koch, C., and Braun, J. (1999). Attention activates winner-take-all competition among visual filters. Nat. Neurosci., *2*, 375–381. 10.1038/7286.
36. Huang, L., and Dobkins, K.R. (2005). Attentional effects on contrast discrimination in humans: evidence for both contrast gain and response gain. Vision Res., *45*, 1201–1212. 10.1016/j.visres.2004.10.024.
37. Ling, S., and Carrasco, M. (2006). Sustained and transient covert attention enhance the signal via different contrast response functions. Vision Res., *46*, 1210–1220. 10.1016/j.visres.2005.05.008.
38. Lee, D.K., Koch, C., and Braun, J. (1997). Spatial vision thresholds in the near absence of attention. Vision Res., *37*, 2409–2418. 10.1016/S0042-6989(97)00055-2.
39. Carrasco, M., Williams, P.E., and Yeshurun, Y. (2002). Covert attention increases spatial resolution with or without masks: Support for signal enhancement. J. Vis. *2*, 467–479. 10.1167/2.6.4.
40. Golla, H., Ignashchenkova, A., Haarmeier, T., and Thier, P. (2004). Improvement of visual acuity by spatial cueing: a comparative study in human and non-human primates. Vision Res., *44*, 1589–1600. 10.1016/j.visres.2004.01.009.
41. Yeshurun, Y., and Carrasco, M. (1998). Attention improves or impairs visual performance by enhancing spatial resolution. Nature, *396*, 72–75. 10.1038/23936.
42. Yeshurun, Y., and Carrasco, M. (1999). Spatial attention improves performance in spatial resolution tasks. Vision Res., *39*, 293–306. 10.1016/S0042-6989(98)00114-X.

43. Carrasco, M., and McElree, B. (2001). Covert attention accelerates the rate of visual information processing. Proc. Natl. Acad. Sci. USA, *98*, 5363–5367. 10.1073/pnas.081074098.
44. Morgan, M.J., Ward, R.M., and Castet, E. (1998). Visual search for a tilted target: Tests of spatial uncertainty models. Q. J. Exp. Psychol. H.E.P., *51A*, 347–370. 10.1080/027249898391666.
45. Palmer, J. (1994). Set-size effects in visual search: The effect of attention is independent of the stimulus for simple tasks. Vision Res., *34*, 1703–1721. 10.1016/0042-6989(94)90128-7.
46. Shiu, L., and Pashler, H. (1994). Negligible effect of spatial precuing on identification of single digits. J. Exp. Psychol. Hum. Percept. Perform., *20*, 1037–1054. 10.1037/0096-1523.20.5.1037.
47. Shiu, L.-P., and Pashler, H. (1995). Spatial attention and vernier acuity. Vision Res., *35*, 337–343. 10.1016/0042-6989(94)00148-F.
48. Cohn, T.E., and Lasley, D.J. (1974). Detectability of a luminance increment: Effect of spatial uncertainty*. J. Opt. Soc. Am., JOSA *64*, 1715–1719. 10.1364/JOSA.64.001715.
49. Dosher, B.A., and Lu, Z.-L. (2000). Noise Exclusion in Spatial Attention. Psychol. Sci., *11*, 139–146. 10.1111/1467-9280.00229.
50. Cheal, M., and Gregory, M. (1997). Evidence of limited capacity and noise reduction with single-element displays in the location-cuing paradigm. J. Exp. Psychol. Hum. Percept. Perform., *23*, 51–71. 10.1037/0096-1523.23.1.51.
51. Lu, Z.-L., Lesmes, L.A., and Dosher, B.A. (2002). Spatial attention excludes external noise at the target location. J. Vis. *2*, 312–323. 10.1167/2.4.4.
52. Dosher, B.A., and Lu, Z.-L. (2000). Mechanisms of perceptual attention in precuing of location. Vision Res., *40*, 1269–1292. 10.1016/S0042-6989(00)00019-5.
53. Lu, Z.L., and Dosher, B.A. (2000). Spatial attention: different mechanisms for central and peripheral temporal precues? J. Exp. Psychol. Hum. Percept. Perform., *26*, 1534–1548. 10.1037//0096-1523.26.5.1534.
54. Pentland, A. (1980). Maximum likelihood estimation: The best PEST. Percept. & Psycho., *28*, 377–379. 10.3758/BF03204398.
55. Prins, N., and Kingdom, F.A.A. (2018). Applying the Model-Comparison Approach to Test Specific Research Hypotheses in Psychophysical Research Using the Palamedes Toolbox. Front. Psychol., *9*. 10.3389/fpsyg.2018.01250.
56. Müller, N.G., Mollenhauer, M., Rösler, A., and Kleinschmidt, A. (2005). The attentional field has a Mexican hat distribution. Vision Res., *45*, 1129–1137. 10.1016/j.visres.2004.11.003.

Methods

Participants

Nineteen participants were recruited for this experiment (11 female, age M ± SD = 23.26 ± 3.80 years; range 18-31). Two participants were excluded from the analyses because they did not complete the full experiment and two because they did not manage to perform the task. All participants had normal or corrected-to-normal vision and reported no history of psychiatric or neurological disorders, gave their written informed consent and were compensated for their participation. All procedures were approved by the French ethics committee Ouest IV - Nantes (IRB #20.04.16.71057) and followed the Code of Ethics of the World Medical Association (Declaration of Helsinki).

Apparatus and stimuli

Participants sat in a dark room at 57cm from a calibrated and linearized CRT monitor (800*600 pixels, width = 37.8cm, height = 28.4cm, refresh rate 120Hz). Their heads were positioned on a chin rest to maintain the distance between the monitor and the eyes. Stimuli were generated using PsychToolbox 3 in Matlab R2018b (MathWorks). Background was gray (127.5, 127.5, 127.5 RGB). A black central fixation annulus with inner eccentricity of 0.2° (degree of visual angle) and thickness of 0.16° was presented throughout the experiment. The cue and response cue were white rectangles (255, 255, 255 RGB, 0.5° long, 0.16° large) adjacent to the fixation (0.65° eccentricity from the center) and pointing down with a 45° angle toward the bottom left or bottom right. Stimuli were two conventional Landolt-C optotypes (2° high, 2° wide, 5.5° from the center at 45° angle toward the left or the right), and randomly generated noise patches at the same locations (2° high, 2° wide; circular window) with or without embedded Gabors (3 cycles per degree; circular window).

Eye-tracking

The dominant eye of each participant was monitored using an infrared video camera (EyeLink 1000 plus, SR Research, Ottawa, Canada). Participants were instructed to maintain fixation. Trial started when they were fixating, and they had to maintain fixation until after the probe presentation. If a fixation break occurred, i.e., if participants' gaze deviated by >1.5° or if they blinked, the trial was stopped and removed from the analysis. Supernumerary trials were added at the end of each block to compensate for rejected trials (M ± SD = 2257.73 ± 1320.76 fixation breaks total on average across participants).

Procedure

Participants performed a total of 22 sessions. First, in a 1h-training session they were familiarized with the trial sequence at slower delays. They then performed two staircase blocks (see below) in an additional 1h-session. They finally performed 20 1h-long sessions (over several days) of the main task.

Main task. Each session was composed of 4 blocks of 126 trials each as well as supernumerary trials in case of fixation break (see **Eye-tracking** section). Central fixation remained on the screen during the entire block. After a 1000ms-stable fixation a pre-cue appeared for 60ms followed by a 400ms-inter-stimulus interval (ISI). The two Landolt-Cs were displayed for 60ms (one in each lower quadrant) along with a response cue indicating which of the two was the target. Participants were instructed to discriminate the position of the C gap (left/right) of the target Landolt-C (their response was collected at the end of the trial sequence). When the target appeared at the cued location (2/3 of the trials), the trial was valid; otherwise (1/3 of the trials) the trial was invalid. Then a second, variable ISI (randomly chosen among 14 different possibilities equally distributed between 40ms and 495ms) preceded the presentation of two new stimuli, i.e., two patches of noise or noise+Gabor for 33ms, at the same location as the previous Landolt-Cs, followed by a 60ms delay. Participants were

instructed to detect the presence/absence of the Gabor inside each patch of noise (50%). These patches presented at multiples delays after the previous Landolt-Cs were used to probe the state of attention across time. At the end of the trial, participants were first asked to report the position of the gap in the target Landolt-C (press C key for a gap on the left with the left hand, and press B key for a gap on the right with the right hand; maximum response time of 1500ms), and then to report the presence or the absence of the Gabor inside each patch (for left patch, press C key for Gabor present and D key for Gabor absent with left hand; for right patch, press B key for Gabor present and H key for Gabor absent with right hand; maximum response time 2000ms).

Staircases. Two independent staircases were implemented via a Best PEST procedure[54] using the Palamedes toolbox[55] in Matlab, to adapt first the size of the Landolt-C gap in the discrimination task, and second the SNR (signal- (Gabor) to-noise ratio) for the detection task. In the first staircase (208 trials), only the discrimination task sequence was presented and the size of the Landolt-Cs gap (1.4 ± 0.4° on average across participants) was adjusted according to a running-fit estimation (Best PEST) of the alpha parameter of a Weibull distribution, corresponding to the gap-size threshold reaching between 70% and 80% performance accuracy (76 ± 2.5% across participants). Here the trial sequence consisted of a neutral pre-cue (both the left and right cue) for 60ms, a 400ms-ISI and the Landolt-Cs together with the response cue for 60ms. Participants had 1.5s to report the location of the gap. In the second staircase (200 trials), the procedure was the same. Only the detection task sequence was presented and the ratio between noise and Gabor was adapted to reach around 50% performance (28 ± 6.9% across participants; note that this staircase was not successful at reaching 50% but there is no reason to presume this impacts the analysis). One trial consisted of neutral pre-cue for 60ms, a 400ms-ISI and the 2 probe patches (50% noise only and 50% noise+Gabor, at each location) with a response cue for 33ms. Participants had 2s to report the presence or the absence of the Gabor in each of the two patches.

Analysis

Behavioral rhythms. All analyses were performed on subsampled trials (100 repetitions) to equalize the number of valid trials to the number of invalid ones. For the discrimination task, performance was evaluated as per d-prime in each cueing condition. We also checked reaction times from Response 1 screen onset (**Figure 1**) to control for speed-accuracy trade-off. Paired samples t-tests were performed to assess statistical differences between cueing conditions.

For the detection task, normalized d-primes were examined for each cueing (valid and invalid) and ISI (delay between the Landolt-C and the probe patches) condition. Responses to both patches were combined. In total, there were 720 trials per ISI and participant. Fast Fourier Transform decompositions (FFT) were further performed on averaged d-primes to assess possible periodicity. Phase angles were extracted from FFTs performed on each participants data for 12.3Hz in valid and 6.1Hz in invalid. We selected high- and low-performance trials by taking local maxima (above d-prime average) and minima (below d-prime average) for each of the d-prime time courses (ISI Valid high: 145, 285, 390 and 460ms; low: 75, 180, 320, 425 and 495ms; ISI invalid high: 110, 320 and 425ms; low: 40, 145, 390 and 460ms). Two local maxima were removed, one in each condition, because they were below the averaged d-primes. All analyses described below were done separately for the high- and low-performance trials.

Reverse Correlation analysis. To perform this analysis, we subsampled (100 repetitions) the number of high- (or low-) performance trials (separately for valid and invalid conditions) to equalize to the number of low- (or high-) performance trials. To address behavioral feature tuning, we first transformed the noise from luminance intensity into the energy of different orientation components. We converted the noise image of each trial from pixel space (luminance intensity of each pixel) to a 1D space defined by the noise energy of components responding to different orientations (varied across all of orientation space, -90° to 90°, in steps of 7.5°, for 25 points on a linear scale). To compute the energy of each component, we took

the noise image $\boldsymbol{S}$ of each trial, and convolved it with two grating filters ($g_{\theta,sin}$ in sine phase and $g_{\theta,cos}$ in cosine phase) with the corresponding orientation. The energy was computed as:

$$\boldsymbol{E_\theta} = \sqrt{(\boldsymbol{S} * \boldsymbol{g_{\theta,sin}})^2 + (\boldsymbol{S} * \boldsymbol{g_{\theta,cos}})^2} \quad (\boldsymbol{Eq1})$$

in which * represents the cross-correlation operator. We took the energy centered at the test stimulus (vertical orientation) for analysis. For each component with preferred orientation θ, we estimated the correlation between the energy of that component and behavioral responses using a GLM to predict the binomial dependent variable:

$$p(yes) = \psi(\beta_\theta E_\theta^* + b_\theta) \quad (Eq2)$$

in which $p(yes)$ was the percentage of yes responses in the detection task and ψ was a cumulative normal distribution. Two free parameters β_θ and b_θ were fitted. β_θ represented the correlation between the energy and the behavioral response. A zero β_θ indicated that the energy of that component did not influence participants' responses. b_θ represented a baseline tendency of the participants to respond "present" (i.e., false alarm rate), which was not related to the stimuli. E_θ^* represented the centered and normalized energy of each component. Before applying the GLM, the energy of each component was first sorted into two groups based on whether the target signal was present or absent in each trial, and the mean of the energy was removed for each group. Therefore, we only used the energy fluctuation of the noise relative to the mean, and the energy used for analysis was centered at zero for both target-present and target-absent trials. To let the estimated β_θ be comparable across components, we further normalized the energy across all the trials in each component to have a standard deviation of 1. The estimated sensitivity kernel was a 1D matrix *K* in which $K(\theta) = \beta_\theta$. Before Gaussian fitting, positive and negative orientations' energy were averaged.

$$\mathrm{x}[1] * (\exp(-\frac{(\mathrm{ori} - \mathrm{x}[2])^2}{2 * \mathrm{x}[3]^2}))^{\mathrm{x}[4]} + \mathrm{x}[5] \quad (\mathrm{Eq3})$$

A Gaussian tuning curve was fit to the data (Eq3) for each condition, where ori represented all noise orientation channels (25 orientations). As we were agnostic as to the precise shape of the tuning function, in addition to the single fit (Eq3) –a simple, standard model of feature tuning

–a double Gaussian fit –a "Mexican hat" (Eq4) shape that sometimes arises due to attention[56]– was computed.

$$\text{(Eq4)}\quad x[1]*\left(\exp\left(-\frac{(ori-x[2])^2}{2*x[3]^2}\right)\right)^{x[4]}+x[5]+x[6]*\left(\exp\left(-\frac{(ori-x[2])^2}{2*x[7]^2}\right)\right)^{x[8]}+x[9]$$

AIC corrected (AICc) for small data samples were performed using Python (3.8.1) independently for each condition to compare single and double Gaussian fits. AICc criterion was computed as shown in (Eq5) where k was the number of parameters, *L* the maximized value of the likelihood function and n the number of participants.

$$\text{(Eq5)}\qquad 2k-2\ln(L)+\frac{2k(k+1)}{n-k-1}$$

For each condition, the single fit better explained the results (valid high-performance AICc difference (single fit – double fit) = -18.9; valid low-performance AICc difference = -37.4; invalid high-performance AICc difference = -37.3; invalid low performance AICc difference = -37.4). All further analyses were thus performed with the tuning curve from the single fits.

We assessed the statistical differences between high- and low-performance trials' tuning curves using linear mixed model with R (4.2.2), and specifically, differences in the standard deviation, amplitude and baseline of the tuning curves. Linear models were fitted by maximizing the restricted log likelihood and using a normal distribution function. Performance was used as predictor with 2 levels (high and low) and participants as random effect.

Code Accessibility

All data and analysis code are available on the OSF repository (https://doi.org/10.17605/OSF.IO/CXKBU).